8. Glanzman, D. L. & Krasne, F. B. *J. Neurosci.* **6**, 1560-1569 (1986).
9. Kravitz, E. A. *et al.* in *Model Neural Networks and Behaviour* (ed. Selverston, A. I.) 339-360 (Plenum, New York, 1985).
10. Kravitz, E. A. in *Fast and Slow Chemical Signalling in the Nervous System* (eds Iversen, L. L. & Goodman, E.) 244-259 (Oxford Science, Oxford, 1986).
11. Beltz, B. S. & Kravitz, E. *J. Neurosci.* **7**, 533-546 (1987).
12. O'Shea, M. & Bishop, C. A. *J. Neurosci.* **2**, 1241-1251 (1982).
13. O'Shea, M. in *Model Neural Networks and Behaviour* (ed. Selverston, A. I.) 401-413 (Plenum, New York, 1985).
14. Bishop, C. A., Wine, J. J., Nagy, F. & O'Shea, M. R. *J. Neurosci.* **7**, 1769-1779 (1987).
15. Otsuka, M., Kravitz, E. A. & Potter, D. D. *J. Neurophysiol.* **30**, 725-752 (1967).
16. Usherwood, D. N. R. & Cull-Candy, S. G. in *Insect muscle* (ed. Usherwood, D. N. R.) 207-280 (Academic, London, 1975).
17. Bicker, G., Schäfer, S., Ottersen, O. P. & Storm-Mathisen, J. *J. Neurosci.* **8**, 2108-2122 (1988).
18. Selverston, A. I., Miller, J. P. & Wadepuhl, M. in *Symp. Soc. exp. Biol.* (ed. Roberts, A. & Roberts, B. L.) 55-87 (Cambridge University Press, Cambridge, 1983).
19. Marder, E. E., Hooper, S. L. & Eisen, J. S. in *Synaptic Function* (eds Edelman, G. M., Gall, W. E. & Cowan, W. M.) 305-327 (Wiley, New York, 1987).
20. Hooper, S. L. & Marder, E. *J. Neurosci.* **7**, 2097-2112 (1987).
21. Heinzel, H. G. *J. Neurophysiol.* **59**, 551-565 (1988).
22. Sombati, S. & Hoyle, G. *J. Neurobiol.* **15**, 481-506 (1984).
23. Stevenson, P. A. & Kutsch, W. *Naturwissenschaften* **73**, 741-743 (1986).
24. Whim, M. D. & Evans, P. D. *J. exp. Biol.* **134**, 247-266 (1988).
25. Malamud, J. G., Mizisin, A. P. & Josephson, R. K. *J. comp. Physiol.* A **162**, 827-835 (1988).
26. Orchard, I. *J. Insect Physiol.* **33**, 451-463 (1987).
27. Hoyle, G. *J. exp. Zool.* **193**, 433-439 (1975).
28. Evans, P. D. & O'Shea, M. *J. exp. Biol.* **73**, 235-260 (1978).
29. Konings, P. N. M. *et al. Cell Tissue Res.* **251**, 371-379 (1988).
30. Goodman, C. S. & Spitzer, N. C. *Nature* **280**, 208-214 (1979).
31. Hoyle, G. & Dagan, D. *J. Neurobiol.* **9**, 59-79 (1978).
32. Shimizu, T. & Fukamii, J. I. *Int. Pest Control* **23**, 166-175 (1981).
33. Linn, C. E. & Roelofs, W. L. *Archs Insect. Biochem. Physiol.* **3**, 161-171 (1986).
34. Stone, B. F. *et al. Pesticide Biochem. Physiol.* **4**, 407-416 (1974).
35. Long, T. F. & Murdock, L. L. *Proc. natn. Acad. Sci. U.S.A.* **80**, 4159-4163 (1983).
36. Long, T. F., Edgecomb, R. S. & Murdock, L. L. *Comp. Biochem. Physiol.* **83c**, 201-209 (1986).
37. Keyserlingk, H. v. *Agric. Zool. Rev.* **1**, 197-254 (1986).
38. Dudai, Y., Buxbaum, J., Corfas, G. & Ofarim, M. *J. comp. Physiol.* A **161**, 739-746 (1987).
39. Erber, J. & Kaulen, P. in *New Frontiers in Brain Research* 247L (eds Elsner, N. & Creutzfeld, O.) (Thieme, Stuttgart, 1987).
40. Classen, D. E. & Kammer, A. E. *J. Neurobiol.* **17**, 1-14 (1986).
41. Loher, W. & Huber, F. *J. Insect Physiol.* **10**, 13-36 (1964).
42. Robinson, G. E. in *Neurobiology and Behavior of Honeybees* (eds Menzel, R. & Mercer, A.) 226-279 (Springer, Berlin, 1987).
43. Truman, J. W. & Weeks, J. C. in *Model Neural Networks and Behavior* (ed. Selverston, A. I.) 381-399 (Plenum, New York, 1985).
44. Tublitz, N. J., Copenhaver, P. T., Taghert, P. H & Truman, J. W. *Trends Neurosci.* **9**, 359-363 (1986).
45. Morton, D. B. & Truman, J. W. *Nature* **323**, 246-267 (1986).
46. Morton, D. B. & Truman J. W. *J. Neurosci.* **8**, 1338-1345 (1988).
47. Levine, R. B. *Trends Neurosci.* **9**, 315-319 (1986).
48. Dunn, A. J. *A. Rev. Psychol.* **31**, 343-390 (1980).
49. Hunter, B. *et al.* in *Handbook of Psychopharmocology* vol 8 *Drugs, Transmitters & Behavior* (eds Iverson, L., Iverson, S. & Snyder, S.) 531-577 (Plenum, New York, 1977).
50. Mason, S. T. *Prog. Neurobiol.* **16**, 263-303 (1981).
51. Kandel, E. R. *et al.* in *Synaptic Function* (eds. Edelman, G. M., Gall, W. E. & Cowan, W. M.) 471-518 (Wiley, New York, 1987).
52. Crow, T. & Forrester, J. *Proc. natn. Acad. Sci. U.S.A.* **83**, 7975-7978 (1986).
53. Tempel, B. L., Livingstone, M. S. & Quinn, W. G. *Proc. natn. Acad. Sci. U.S.A.* **81**, 3577-3581 (1984).
54. Tully, T. *Trends Neurosci.* **10**, 330-335 (1987).
55. Kety, S. S. in *The Neuroscience Second Study Program* (ed. Schmitt, F. O.) 324-336 (Rockfeller University Press, New York, 1970).
56. McGaugh, J. L. *A. Rev. Physchol.* **34**, 297-323 (1983).
57. Menzel, R. *Naturwissenschaften* **70**, 504-511 (1983).
58. Menzel, R. & Michelsen, B. in *Learning and Memory: Mechanisms of Information Storage in the Nervous System* (ed. Matthies, H.) 273-275 (Pergamon, Oxford, 1986).
59. Mercer, A. R. & Menzel, R. *J. comp. Physiol.* **145**, 363-268 (1982).
60. Macmillan, C. S. & Mercer, A. R. *J. comp. Physiol.* A **160**, 359-366 (1987).
61. Michelsen, D. B. *Comp. Biochem. Physiol.* C (In the press).
62. Menzel, R., Michelsen, B., Rüffer, P. & Sugawa, M. in *Modulation of Synaptic Transmission and Plasticity in Nervous Systems* (eds Hertting, G. & Spatz, H. Ch.) 333-349 (Springer, Berlin, 1988).
63. Bitterman, M. E., Menzel, R., Fietz, A. & Schäfer, S. *J. comp. Physiol. Psychol.* **97**, 107-119 (1983).
64. Kuwabara, M. *J. Fac. Sci. Hokkaido Univ. Series* 6, *Zoology* **13**, 458-464 (1957).
65. Menzel, R., Erber, J. & Masuhr, Th. in *Experimental Analysis of Insect Behavior* (ed. Barton-Browne, L.) 195-217 (Springer, New York, 1974).
66. Erber, J., Masuhr, Th. & Menzel, R. *Physiol. Entomol.* **5**, 343-358 (1980).
67. Huber, F. in *Invertebrate Nervous Systems* (ed. Wiersma, C. A. G.) 333-351 (University of Chicago Press, Chicago, 1967).
68. Rehder, V., Bicker, G. & Hammer, M. *Cell Tissue Res.* **247**, 59-66 (1987).
69. Kupfermann, I. & Weiss, K. R. in *Serotonin, Neurotransmission and Behavior* (eds Jacobs, B. L. & Gelperin, A.) 225-287 (M.I.T. Press, Cambridge, Massachusetts, 1981).
70. Lent, C. M. & Dickinson, M. H. *J. comp. Physiol.* A **154**, 457-471.
71. Altman, J. S. & Kien, J. in *Arthropod Brain* (ed. Gupta, A. P.) 265-301 (Wiley, New York, London, 1987).
72. Nässel, D. R. *Prog. Neurobiol.* **30**, 1-85 (1988).
73. Tyrer, N. M., Turner, J. D. & Altman, J. S. *J. comp. Neurol.* **227**, 313-330 (1984).
74. Mobbs, P. G. *Phil. Trans. R. Soc.* B **298**, 309-354 (1982).

ARTICLES

A unique geochemical record at the Permian/Triassic boundary

William T. Holser*, Hans-Peter Schönlaub†, Moses Attrep Jr‡, Klaus Boeckelmann§, Peter Klein†, Mordeckai Magaritz‖, Charles J. Orth‡, Alois Fenninger¶, Catherine Jenny#, Martin Kralik, Hermann Mauritsch††, Edwin Pak‡‡, Josef-Michael Schramm§§, Karl Stattegger¶ & Rupert Schmöller††**

* Department of Geological Sciences, University of Oregon, Eugene, Oregon 97403, USA
† Geologische Bundesanstalt, Postfach 154, A-1031 Wien, Austria
‡ Isotope and Nuclear Chemistry Division, Los Alamos National Laboratory, Los Alamos, New Mexico 87545, USA
§ Institut für Geologie und Paläontologie, Technische Universität Berlin, Ernst-Reuter-Platz 1, D-1000 Berlin 10, FRG
‖ Isotope Research Department, The Weizmann Institute, Rehovot 76100, Israel
¶ Institut für Geologie und Paläntologie, Karl-Franzens-Universität Graz, Heinrichstrasse 26, A-8010 Graz, Austria
# Musée géologique cantonal, UNIL-BFSH-2, CH-1015 Lausanne, Switzerland
** Geotechnisches Institut, BVFA Arsenal, A-1030 Wien, Austria
†† Institut für Geophysik, Montanuniversität Leoben, Franz-Josef-Strasse 18, A-8700 Leoben, Austria
‡‡ Institut für Radiumforschung und Kernphysik, Universität Wien, Boltzmanngasse 3, A-1090 Wien, Austria
§§ Institut für Geowissenschaften, Universität Salzburg, Akademiestrasse 26, A-5020 Salzburg, Austria

A 330-metre core drilled through the marine Permian/Triassic boundary in the Carnic Alps of Austria allows closely correlated studies of geochemistry, petrography and palaeontology across the boundary. The isotope shifts and metal concentrations are extended, multiple and complex, and do not resemble those seen at the Cretaceous/Tertiary boundary. Both the carbon isotope shifts and the chemical events (including an iridium anomaly) may have causes related to a major regression of the sea.

THE Permian/Triassic (P/Tr) boundary is associated with the largest extinction event in Phanerozoic time[1]. It also witnessed important changes in the environment[2], notably indicated by a large drop in $\delta^{13}C$ of the surface ocean from the relatively enriched ^{13}C condition that characterized the late Palaeozoic[3,4]. A sudden decrease in $\delta^{13}C$ has also been observed in connection with other extinction events: the Precambrian/Cambrian[5], Ordovician/Silurian[6], Frasnian/Famennian[7], Devonian/Car-

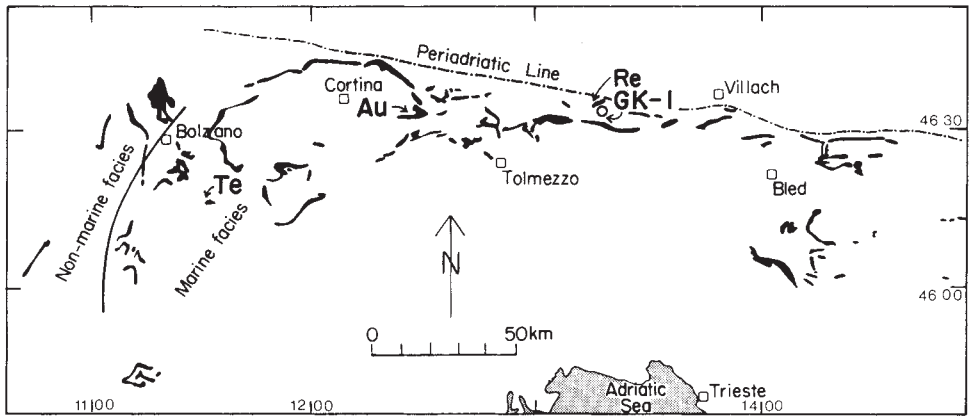

Fig. 1 Location of the Gartnerkofel-1 (GK-1) core hole in relation to the surface distribution of P/Tr rocks in the southern Alps[31]. Also shown are locations of the outcrop sections at the nearby Reppwand (Re), and at Tesero (Te) and Auronzo (Au), Italy[28]. The GK-1 locality is on a gently dipping marine shelf, 160 km east of the shoreline near Bolzano, Italy.

boniferous[8], Cenomanian/Turonian[9] and Cretaceous/Tertiary (K/T)[10]. At some of these boundaries, anomalous concentrations of metals, particularly iridium, have been observed. The high concentrations at the K/T boundary[11] and the more modest but distinct concentrations in the Late Eocene[12] have been widely ascribed to bolide impacts, whereas concentrations at some of the other extinction events[7,13–17], similar to those in the Late Eocene, may have been caused by terrestrial processes (biogenic, oceanic or volcanic).

Suggestions of iridium anomalies associated with the P/Tr boundary have been controversial. Notable iridium anomalies have been reported at exposures of the P/Tr boundary in China[16–19], but analyses of these same sections in other laboratories have failed to find iridium concentrations of more than 100 parts per 10^{12} (refs 20–23). Similarly low levels of iridium were found in P/Tr sections in Soviet Armenia[24] and in the Dolomite Alps[25,26].

Our objective in the current study has been to completely characterize the geochemistry and palaeoenvironment of a representative section of the P/Tr boundary, including carbon isotope and iridium characteristics as well as other measures, and to compare the conditions near the boundary with those in the contiguous sections of the Upper Permian and Lower Triassic.

The Gartnerkofel core

Previous studies of carbon isotope profiles of the P/Tr boundary have indicated that some of the most complete sections across the boundary were situated in the Southern Alps of Austria and Italy[27–29]. To obtain the best possible reference section free of any outcrop alteration, a continuous core was taken specifically for this purpose, on the north slope of the Gartnerkofel near Nassfeld in the Carnic Alps of Austria (Fig. 1). This locality was near the western end of the Tethys Sea, on a carbonate ramp gently inclined to the south-east and 160 km east of the shoreline exposed in the western Dolomite Alps[30,31]. Hole GK-1 started in the Muschelkalk Conglomerate (Upper Anisian), entered the Werfen Formation (Skythian) at 57 m, the Bellerophon Formation (Dzhufian–Dorashamian) at 231 m, and bottomed in the same formation at 331 m (Fig. 2). Oolites in the lowermost 6 m of the Werfen Formation correlate with the Tesero Horizon in the Italian Dolomites, where the P/Tr boundary, as defined by the last occurrence of Permian fusulinids[32–34], lies within this Tesero Horizon. In both GK-1 and the nearby outcrop on the Reppwand cliffs, conodonts were recovered from the lower 40 m of the Werfen Formation. The recognition of *Hindeodus parvus*, a conodont guide fossil for the Early Griesbachian[35,36], confirms a very thick and complete representation of lowermost Triassic sediments at this locality. The palaeomagnetic record in the core displays several polarity reversals, as seen in the Permo-Triassic Mixed (Illawarra) Superchron. The reversal nearest to the P/Tr boundary, from positive to negative polarity, lies within the Upper Permian (at 237.2 m); an analogous reversal in the P/Tr section at Shangsi, China, is close to the boundary within a sampling gap of 1.5 m (ref. 37).

The absolute time interval corresponding to the stratigraphic units outlined in Fig. 2 is difficult to assess. Units 1B to 3B—constituting a thickness of ~200 m—correspond to probably not more than one stage each of the Permian (Dorashamian) and Triassic (Griesbachian)[38], a time interval of ~5 Myr (ref. 39). This rate of ~40 m Myr^{-1} is equal to that calculated for the section at Shangsi[37], and is within the expected range for carbonate shelf sedimentation[40].

Closely coordinated sampling of the core allows comparison of a wide variety of data. About 300 billets were cut for thin-section preparation; the remainders of these billets were milled to powder and split for mineralogical, chemical and isotope analyses. Every one of the shaly or marly interbeds, about 50 in number and mostly a few millimetres thick, was similarly sampled and analysed. Samples were spaced in most of the core at a maximum distance of ~1 m, but were as close as 10 cm apart in the vicinity of the boundary. The complete scheme of sampling and analysis, and all the analytical results, are to be published elsewhere (W.T.H. *et al.*, to be submitted to *Jb. geol. Bund.*) Some salient features of the results are given here.

Carbon isotopes

The carbon isotope profile of Figs 2 and 3*a* suggests further subdivision of the section. Unit 1A, the middle part of the Bellerophon Formation (from the bottom of the core to 293.5 m), has ^{13}C-enriched values (mean $+3.0 \pm 0.3$‰). These values are within the range of those reported for Upper Permian rocks, both in other sections in the Alps[27,28] and throughout Tethys[29,41]. Unit 1B comprises the upper part of the Bellerophon Formation, where $\delta^{13}C$ values drop gradually from +2.8‰, to +1.5‰ at a depth of 231.3 m, at a rate of 0.02‰ m^{-1}. Comparison of this carbon isotope profile from GK-1 with others to the west at Tesero and Auronzo, Italy (Fig. 1)[28], indicates that this segment in GK-1 corresponds to the sharp drop in $\delta^{13}C$ that occurred within a few tens of centimetres in the Italy sections. In Unit 2 (the Tesero Horizon, which includes the P/Tr boundary) $\delta^{13}C$ continues to drop, reaching a value of 0.0‰ at 224.7 m. This segment has the same values of $\delta^{13}C$ and thickness as those of the Tesero Horizon at Tesero[28,42]. Unit 3A is an interval of low $\delta^{13}C$ in the lower part of the Mazzin Member of the Werfen Formation, extending to 175 m and including three minima, which will be discussed below. This multiple low was not found at any of the other P/Tr sections studied thus far. Units 3B and 4 comprise the upper part of the Werfen Formation, to 57 m, with a constant $\delta^{13}C$ of $+1.3 \pm 0.2$‰.

Oxygen isotopes

Values of $\delta^{18}O$ also show some consistent variations in certain intervals (Fig. 2). In Unit 1A the values of $\delta^{18}O$ show a bimodal distribution, centred at $\delta^{18}O = -0.5$ and -3.0‰, and the less

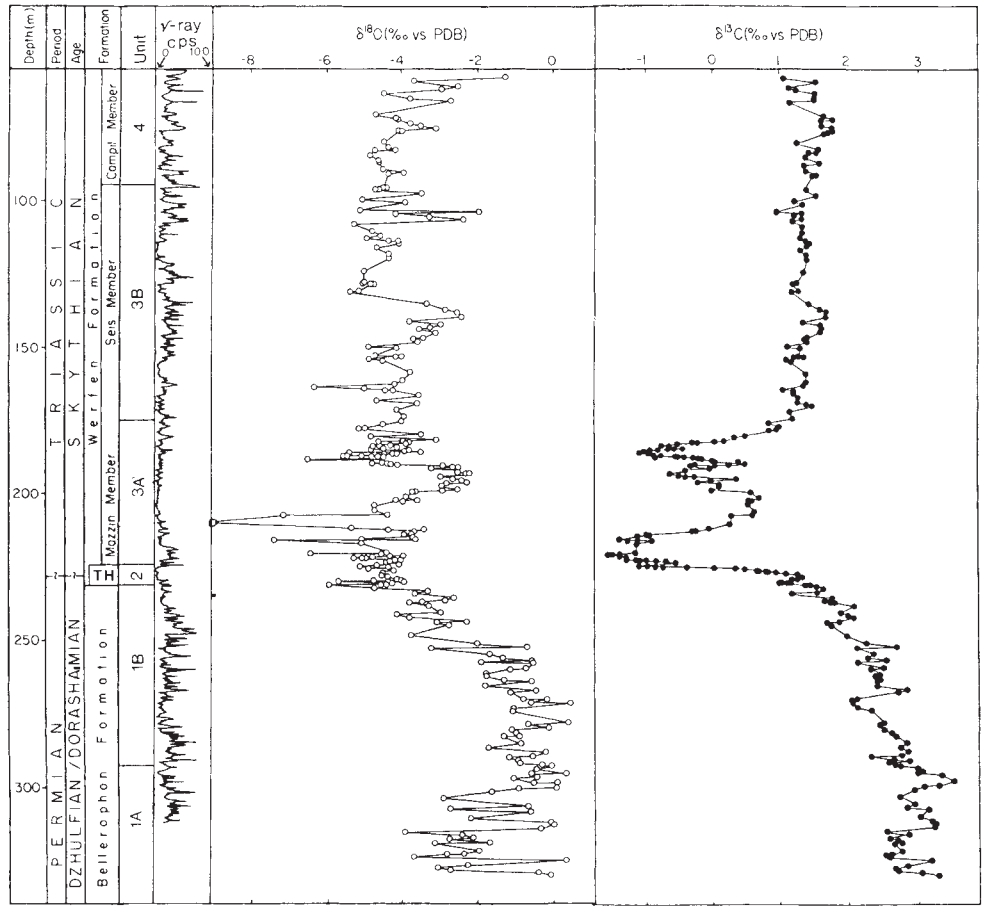

Fig. 2 Stratigraphy, geophysical log, and oxygen and carbon isotopes in GK-1. Four lithostratigraphic units are recognized, with subunits based on carbon isotope shifts. Virtually the entire section is fine-grained dolostone, with occasional millimetre-to centimetre interbeds of dolomitic marl or shale (natural γ-ray log >25 counts per second). Unit 1 is the middle and upper part of the Bellerophon Formation, a low-energy, homogeneous, bioturbated biomicrite of a shallow inner shelf, dominated by foraminifers. Unit 2 (231.0–224.5 m), the Tesero Horizon (TH), is transitional to a more shallow and restricted environment: oolites appear in the upper 4 m, with increasing tempestites, intraclasts, ostracodes and worm tubes. Unit 3 is the lower part of the Lower Triassic Werfen Formation, containing strongly bioturbated microsparite, with increasing coquina tempestites. In the interval 95–82 m the section becomes more red, less fossiliferous and richer in terrestrial clastics that characterize Unit 4. At the top of the section a hiatus of the higher parts of the Werfen Formation is followed at 75 m by the Anisian Muschelkalk Conglomerate (not shown). The clastic residues in Unit 1 are mainly illite/muscovite, whose measured crystallinity[67] attests to only very-low-grade diagenesis (<180 C). Upwards through Unit 3, detrital quartz and minor chlorite become dominant.

negative values continue in the lower part of Unit 1B. More negative $\delta^{18}O$ values of about −3.5‰ occur in the upper part of Unit 1B and persist consistently through Units 2 ($\delta^{18}O = -4.5 \pm 0.5$‰) and Units 3 and 4 ($\delta^{18}O = -4.2 \pm 0.8$‰), despite the substantial variations of $\delta^{13}C$ that characterize those intervals (Fig. 2). The consistent nature of the variations of $\delta^{18}O$ speaks for a mainly primary record of $\delta^{18}O$ in this core section. The depletion of $\delta^{18}O$ across the P/Tr boundary (Units 1 to 2 and 3) may be interpreted as indicative of a temperature rise of perhaps 5 °C.

Stable isotopes and chemistry across P/Tr

Detailed profiles of selected stable-isotope and chemical variations for the interval 235–175 m, which crosses the P/Tr boundary, are displayed in Fig. 3. This interval has complex variations of carbon isotopes and chemistry.

The smooth decrease of $\delta^{13}C$, which starts in Unit 1B, continues through Unit 2 at an accelerating rate, reaching 0.3‰ m^{-1}. This sharp drop in $\delta^{13}C$ signals the beginning of a zone of low $\delta^{13}C$ values, which includes three clear minima at 220 (−1.5‰), 193 (−0.6‰) and 186 m (−1.5‰), until a more stable regime with $\delta^{13}C \approx +1.3$‰ is re-established above 173 m (Fig. 2).

This ^{13}C-depleted zone is also characterized by chemical changes. The first and third carbon isotope minima have high concentrations of pyrite (>500 μmol g^{-1} S_2), as shown by dashed lines in Fig. 3*b*. Total Fe, shown as solid lines in Fig. 3*b*, is nearly matched (in μmol g^{-1}) by S_2 in these two pyritic intervals, underlain in both cases by oxidized intervals low in S_2, with most of the iron as goethite. Pyrite has wavy lamellar bedding consisting of globular masses 20–100 μm in diameter, similar to the early diagenetic 'framboidal' pyrite common in modern marine muds and in stratiform sulphide deposits such as the Kupferschiefer, Meggen and Rammelsberg[43,44]. Each of the stratigraphically distinct sulphide concentrations in Fig. 3*b* has a negative, uniform but distinct isotope ratio: for example, near 186 m, $\delta^{34}S = -19.3 \pm 0.2$‰ and at 221–222 m, $\delta^{34}S = -25.7 \pm 1.1$‰. These data indicate that the pyrite is syngenetic-diagenetic, and that each bed was deposited in its own distinct reducing environment. This conclusion is supported by rare-earth-element chemistry (Fig. 3*c*). Ratios of Ce*/La* have their highest values of ~1.0 in the intervals rich in pyrite, indicating anoxic conditions in the sedimentary regime[45,46]. Immediately below, in the interval 231–225 m, $Ce^*/La^* = 0.5 \pm 0.1$, as would be expected under the highly aereated conditions in which oolites are generated. The rise in Ce*/La* begins immediately above the oolite beds, 2 m below the beds in which considerable pyrite is preserved. Above the sulphide zone, Ce*/La* ratios (in shaly samples) decrease to intermediate values of ~0.7.

The iridium data also show two peaks (normalized to Al in Fig. 3*d*) that are substantially above background. The first (165 parts per 10^{12} Ir ($Ir/Al = 4.15 \times 10^{-9}$)), at the top of Unit 2 (224.5 m), occurs while $\delta^{13}C$ is still declining sharply towards its first minimum and the local conditions are just changing from oxic to anoxic. The second Ir peak (230 parts per 10^{12} ($Ir/Al = 6.80 \times 10^{-9}$)) is near the top of Unit 3A (185.6 m), centred on the third minimum of $\delta^{13}C$ and on a peak of S_2. The highest iridium concentrations are clearly above the relatively low background of iridium (10–30 ± 5 parts per 10^{12} in shaly samples) that apparently characterizes this geological period; they persist whether plotted as Ir/Al (Fig. 3*d*), Ir/Fe or just Ir. They are at least an order of magnitude lower than the iridium spike at the K/T boundary, but are similar to iridium concentrations described near other boundaries[7,13–15]. A log plot of Co against Ir (Fig. 4) shows that Permian/Triassic samples (including both our data from Austria and three analyses from China[21]) have lower Ir than (1) mean CI chondrite[47], (2)

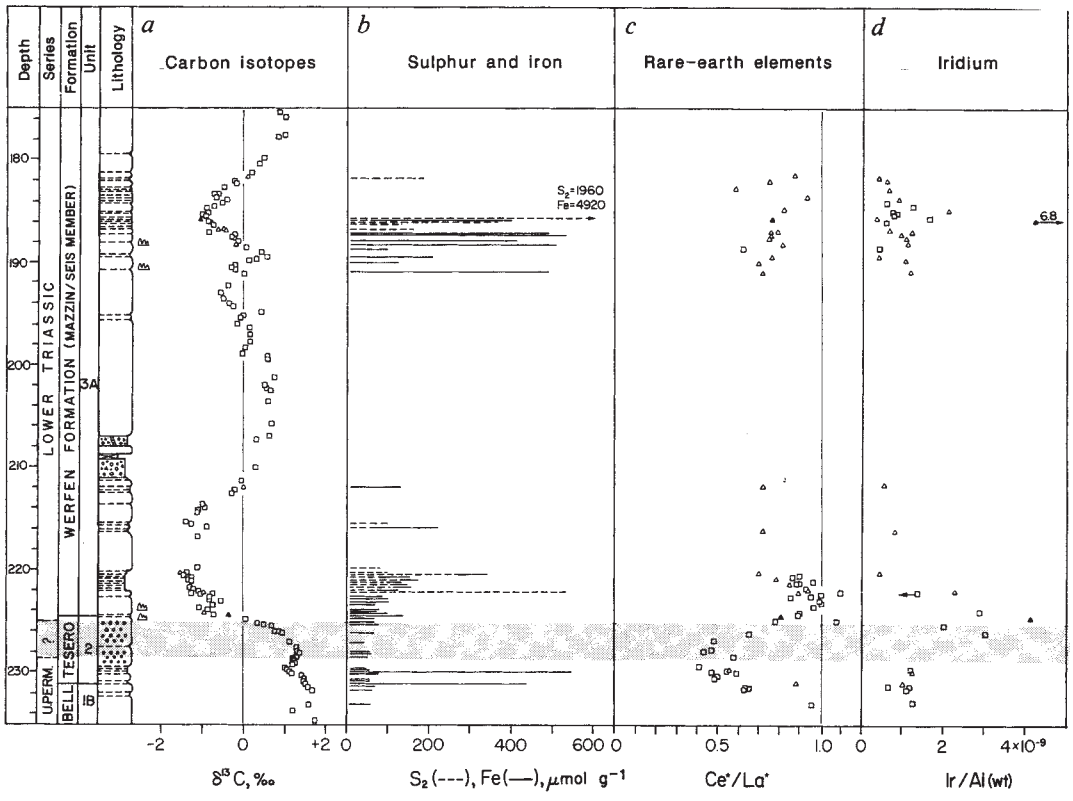

Fig. 3 Details of stratigraphy and geochemistry in GK-1, from 235 to 175 m, across the P/Tr boundary (shaded). Levels with *H. parvus* indicated alongside lithology. Squares represent dolostone, triangles represent shale or marl, and samples of the two iridium spikes are shown as solid symbols. *a*, Carbon isotope profile; note the steep but smooth decline of $\delta^{13}C$ across the P/Tr boundary, and the subsequent three minima in the lowermost Triassic; shale and carbonate samples are consonant. *b*, Total sulphur (nearly all is sulphide; analyses by combustion) and total iron (by instrumental neutron activation analysis (INAA)), expressed in $\mu mol\ g^{-1}$ of S_2 and Fe, respectively. In all cases the Fe is sufficient to indicate that all S appears as pyrite, FeS_2, which displays two peaks. *c*, Rare-earth elements (analysed by INAA), illustrated by Ce*/La*, each normalized to the North American shale composite[68]. Note the shift from low to high ratio (oxidizing to reducing conditions) at the upper boundary of the Tesero oolite. *d*, Iridium (analysed by RNAA), here normalized by its ratio to Al (analysed by INAA). The low background value of this ratio, at $\sim 1 \times 10^{-9}$, is maintained consistently through all the shaly layers and even above and below the section shown here. Two anomalies of many times the background level, at 4 and 7×10^{-9}, are seen at just above the P/Tr stratigraphic boundary as $\delta^{13}C$ passes through zero, and at about 40 m above the P/Tr boundary where $\delta^{13}C$ drops to its third minimum. Each of the two iridium anomalies rises sharply but drops off more slowly, over 1–2 m.

chondritic spherules from the deep sea[48], (3) chondritic spherules from the Tunguska event[49], and (4) peak spikes at the K/T boundary[50–51]. As indicated in Fig. 4, the ratios of Co/Ir in both background and in the nominal peaks of the GK-1 profile are more similar to those found in deep-sea muds[52] and manganese nodules[53,54]. Plots of Ni against Ir and Cr against Ir are similar to plots of Co against Ir.

Three samples from the upper Ir high were also analysed by radiometric neutron activation analysis (RNAA) for Au, and gave Au/Ir = 16, 30 and 56 (weight ratio). These are closer to the ratios found in basalts or kimberlites (summarized by Paul *et al.*[55]) than those in chondrites[47], K/T boundary clays[50] or deep-sea manganese nodules[53].

The weakest carbon isotope minimum (at 193 m; Fig. 3) is in a carbonate interval with no concentration of clay or pyrite, and has not yet been analysed for trace elements by NAA.

Geochemical measures of detrital provenance are constant, with no trend over the whole length of the core: $Th/Al = 0.161 \pm 0.028 \times 10^{-3}$ ($n = 76$) and $Ga/Sc = 1.70 \pm 0.36$ ($n = 25$). The latter ratio[56], and minor olivine and augite in heavy-mineral concentrates in Unit 3, suggest some input of fresh basic volcanic material, such as may have been derived from the Permian/Skythian Haselgebirge of the Northern Calcareous Alps[57].

Ten analyses of strontium isotope ratios ($^{87}Sr/^{86}Sr$) in carbonate rocks between 238 and 185 m (Units 1B, 2 and 3A), corrected for small amounts of radiogenic rubidium, had a mean value of 0.70742 (with a range of 0.70702–0.70777), similar to latest Permian[58] and earliest Triassic[2] rocks of western USA, but with no local evidence of an upward trend.

Modelling chemical changes

Taking into consideration the evidence presented here and that in earlier studies[2,3,28,29], we suggest the following model for changes that occurred in the environment across the P/Tr boundary.

The end of the Permian was characterized by one of the strongest regressions of the sea in the entire Phanerozoic[2], which explains why part of the boundary beds are missing in most of the marine sections around the world. Moreover, the thickness of the section in GK-1 that yields *H. parvus* (Fig. 3*a*) suggests that the Nassfeld area has a rather complete representation of 'boundary beds'. Thus the chemistry of GK-1 provides a very detailed record which substantially constrains the geochemical model.

A major shift in the carbon cycle was initiated early in the Dorashamian stage, based on evidence in sections across Tethys[29]. Thus the drop in $\delta^{13}C$ that begins in GK-1 (at least 50 m below the P/Tr boundary) indicates a net oxidation of the world reservoirs of organic carbon, as sea level dropped, exposing paralic and shallow shelves to erosion. The $\delta^{13}C$ profile in GK-1 confirms an acceleration in the rate of organic carbon oxidation as the boundary is approached, as was seen previously at Tesero, Italy[28]. At both Tesero[42] and in GK-1 (Fig. 3) the occurrence of oolites suggests that the sea had withdrawn to nearly expose these parts of the Tethys shelf.

A sharp change to anoxic conditions is evident at the top of Unit 2 in the GK-1 core by the rise in Ce*/La* and then the appearance of pyrite and high S/C ratios. The inception of anoxia, as $\delta^{13}C$ was dropping through zero for the first time, was marked by anomalous concentrations of iridium and other metals, and the maximum of the anoxic zone corresponds to the initial minimum in the profile of $\delta^{13}C$. A similar sequence is repeated during a later minimum of $\delta^{13}C$ at the top of Unit 3A (185.6 m), which is accompanied by another high concentration of metals and sulphide.

A (single) minimum zone of $\delta^{13}C$ at the base of the Early

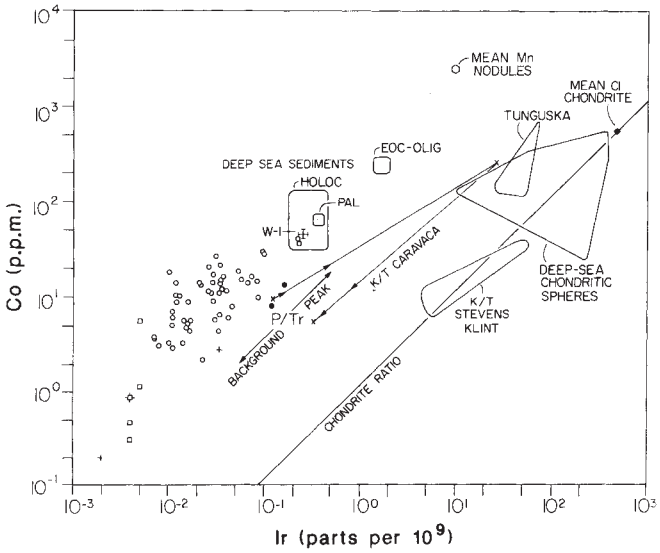

Fig. 4 Plot of cobalt against iridium on a log-log plot. Data from this study (from the Carnic Alps) are indicated as squares (dolostone) or circles (shale or marl); symbols for the two iridium spikes are solid. The data show a general positive correlation, but at a relatively lower Ir value than that for mean CI chondrite[47] or chondritic spherules[48,49]. Shown for comparison are two values for the P/Tr boundary beds in Changxing, China[21] (+), and two examples of the K/T peak (transition through the spike at Caravaca, Spain[50], marked ×, and the range of peak values at Stevens Klint, Denmark[51]). Also shown are approximate ranges of background for Palaeocene and Eocene-Oligocene (ref. 69 and F. T. Kyte and K. T. Wasson, personal communication) and Holocene (Ir: ref. 52; Co: ref. 70) deep-sea sediments, and mean values for manganese nodules (Ir: ref. 53; Co: ref. 54).

Triassic has been verified on a global scale[3,29]. The chemical changes that we see in GK-1—high iridium, other metals, sulphide and cerium—are certainly an important local signal, although they have not yet been found elsewhere. Whether they are local or worldwide, one must ask why these chemical changes have followed so closely upon the primary, worldwide, longer-term shifts of the carbon cycle. The explanation may be that both the carbon isotope shift and the chemical changes were caused by the same regression of sea level, which first exposed organic carbon to oxidation and finally brought about anoxic conditions to precipitate metals in at least this part of the Tethys Sea. This is consistent with increased erosion of upraised red beds[59] and volcanics[60], now exposed west of Bolzano (Fig. 1), bringing metals into solution which were finally reprecipitated on contacting the anoxic waters that had been generated in Tethys. Alternatively, the metals may have been dissolved from the red beds of the underlying Gröden Formation, and precipitated at the oxidation/reduction interface, as has been proposed for the metal-rich (including platinum-group elements) shales of the Kupferschiefer[61–63].

Accumulation of metals may have been aided by algae, whose presence is suggested by the lamellar textures seen in this interval. If detailed investigations of other sections show that anoxia and concentrations of metals are localized in this Bellerophon basin, one might then suggest that the cause is an estuarine-style topflow of the fresh waters from the lands to the west during the maximum regression of the Tethys Sea. Alternatively, on a larger scale it could represent a final phase of a deep-sea oxygen-minimum zone that was prevalent for much of the Palaeozoic[64,65], brought near the surface during this maximum regression. The prevailing incidence of fresh water eroding continental rocks during this period of regression is evidenced by the high values of $^{87}Sr/^{86}Sr$ compared with those of earlier Permian time[2], but we have not seen a short-term positive spike such as that seen at the K/T boundary[66].

Unlike other boundaries, for which a single rather sharp drop in $\delta^{13}C$ is followed by a relatively rapid recovery to normal $\delta^{13}C$, we found in GK-1 a thick section (Unit 3A, about 50 m) of low $\delta^{13}C$, including three separate minima, the two largest of which were characterized by anoxic conditions and enrichment of metals including iridium. Isotope profiles presented previously[28,29] have indicated that important worldwide changes in the carbon cycle had already begun in Late Permian time and continued smoothly across the stratigraphic P/Tr boundary to culminate in the Early Triassic. The detailed study of GK-1 confirms this extended interval of change, and presents a complex picture of oxidation, reduction and metal deposition constrained within the interval of carbon variations. The evidence presented here, from the most dramatic of all mass extinction events, provides a scenario that is completely different from the bolide impact model proposed for the K/T event, and which is less dependent on iridium anomalies. Certainly, a sharp event or events such as are seen at the K/T boundary are not in evidence here.

The geological coring was funded by the Fonds zur Förderung der Wissenschaftlichen Forschung and the NSF under the Austria-USA Cooperative Science Program. Some of the analytical work was supported by the Geologische Bundesanstalt, NASA and the US Department of Energy, and The Weizmann Institute.

Received 5 August; accepted 14 November 1988.

1. Raup, D. M. & Sepkosky, J. J. Jr *Science* **215,** 1501–1503 (1982).
2. Holser, W. T. & Magaritz, M. *Mod. Geol.* **11,** 155–180 (1987).
3. Holser, W. T., Magaritz, M. & Clark, D. L. *Am. J. Sci.* **286,** 390–402 (1986).
4. Popp, B. N., Anderson, T. F. & Sandberg, P. A. *Bull. geol. Soc. Am.* **97,** 1262–1269 (1986).
5. Magaritz, M., Holser, W. T. & Kirschvink, J. L. *Nature* **320,** 258–259 (1986).
6. Orth, C. J., Gilmore, J. S., Quintana, L. R. & Sheehan, P. M. *Geology* **14,** 433–436 (1986).
7. Playford, P. E., McLaren, D. G., Orth, C. J., Gilmore, J. S. & Goodfellow, W. D. *Science* **226,** 437–439 (1984).
8. Xu, D.-Y. *et al. Nature* **321,** 854–855 (1986).
9. Kauffman, E. G., Elder, W. P. & Pratt, L. M. in *3rd Int. Conf. on Global Bioevents: Abrupt Changes in the Global Biota* 22 (Univ. Colorado, Boulder, 1988).
10. Margolis, S. V., Mount, J. F., Doehne, E., Showers, W. & Ward, P. *Paleoceanography* **2,** 361–377 (1987).
11. Alvarez, W., Alvarez, L. W., Asaro, F. & Michel, H. V. *Geol. Soc. Am. spec. Pap.* **190,** 305–315 (1982).
12. Keller, G. *et al. Meteoritics* **22,** 25–60 (1987).
13. Orth, C. J. *et al. Geology* **16,** 627–630 (1988).
14. Orth, C. J., Quintana, L. R., Gilmore, J. S., Grayson, R. C. Jr & Westergaard, E. H. *Geology* **14,** 986–990 (1986).
15. Orth, C. J. *Geophys. Res. Lett.* **15,** 346–349 (1988).
16. Sun, Y. *et al. 27th Int. geol. Cong. Abstr.* **8,** 309–310 (1984).
17. Xu, D.-Y. *et al. Nature* **314,** 154–156 (1985).
18. Chai, C. *et al. Dizhixue Bao* [*Acta Geol. Sinica*] **60,** 139–150 (1986).
19. Sun, Y.-Y., Xu, D.-Y., Yan, Z. & Chai, Z. F. *Ber. geol. Bund. (Wien)* **15,** 29–30 (1988).
20. Asaro, F., Alvarez, L. W., Alvarez, W. & Michel, H. V. *Geol. Soc. Am. spec. Pap.* **190,** 517–528 (1982).
21. Clark, D. L., Wang, C.-Y., Orth, C. J. & Gilmore, J. S. *Science* **233,** 984–986 (1986).
22. Zhou L. *Geol. Soc. Am. Abstr. Prog.* **19,** 904 (1987).
23. Boclet, D., Baud, A., Bonté, P., Jéhanno, C. & Rocchia, R. *C. R. Acad. Sci. Paris* **307,** 261–266 (1988).
24. Alekseev, A. S., Barsukova, L. D., Kolesov., G. M., Nazarov, M. A. & Grigoyan, A. G. *Lunar planet. Sci.* **14,** 7–8 (1983).
25. Oddone, M. & Vannucci, R. in *Field Conference on Permian and Permian-Triassic Boundary in the South Alpine Segment of the Western Tethys, Field Guidebook* 28–29 (Soc. Geol. Italia, Brescia, Italy, 1986).
26. Brandner, R. *Ber. geol. Bund. (Wien)* **15,** 49–56 (1988).
27. Holser, W. T. & Magaritz, M. *Jb. geol. Bund. (Wien)* **128,** 75–82 (1985).
28. Magaritz, M., Bär, R., Baud, A. & Holser, W. T. *Nature* **331,** 337–339 (1988).
29. Baud, A., Magaritz, M. & Holser, W. T. *Geol. Rundschau* (in the press).
30. Buggisch, W. *Carinthia II* **164,** 17–26 (1974).
31. Buggisch, W. *Geol. Rundsch.* **67,** 149–180 (1978).
32. Neri, C. & Passini, M. *Boll. Soc. paleont. Ital.* **23,** 113–117 (1985).
33. Noé, S. *Facies* **16,** 89–142 (1987).
34. Passini, M. *Riv. Ital. Paleont. Stratigr.* **90,** 481–510 (1985).
35. Kozur, H. *Freiberger Forsch.* C**344,** 85–161 (1978).
36. Sheng, J.-Z. *et al. J. Fac. Sci. Hokkaido Univ. Ser.* 4 **21,** 133–181 (1984).
37. Heller, F., Lowrie, W., Li H, & Wang J. *Earth planet. Sci. Lett.* **88,** 348–356 (1988).
38. Broglio Loriga, C., Neri, C. & Posenato, R. in *Field Conference on Permian and Permian-Triassic Boundary in the South-Alpine Segment of the Western Tethys, Field Guide-Book* 29–34 (Soc. Geol. Ital., Brescia, Italy, 1986).
39. Haq, B. U., Hardenbol, J. & Vail, P. R. *Science* **235,** 1156–1169 (1987).
40. Scholle, P. A., Arthur, M. A. & Edkale, A. A. *Mem. Am. Ass. Petrol. Geol.* **33,** 620–691 (1983).
41. Chen, J., Shao, M., Huo, W. & Yao, Y. *Sci. Geol. Sinica 1984 (1)* 88–93 (1984).
42. Neri, C., Pasini, M. & Posenato, R. in *Field Conference on Permian and Permian-Triassic Boundary in the South Alpine Segment of the Western Tethys, Field Guide-Book* 123–128 (Soc. Geol. Ital., Brescia, Italy, 1986).
43. Love, W. G. & Amstutz, G. C. *Fortschr. Miner.* **43,** 273–309 (1966).
44. Ostwald, J. & England, B. M. *Miner. Mag.* **43,** 297–300 (1979).
45. Freyer, B. J. *Geochim. cosmochim. Acta* **41,** 361–367 (1977).
46. Wright, J., Schrader, H. & Holser, W. T. *Geochim. cosmochim. Acta* **51,** 631–644 (1987).
47. Wasson, J. T. *Meteorites—Their Record of Early Solar-system History* (Freeman, New York, 1985).

48. Bonté, P., Jéhanno, C., Maurette, M. & Brownlee, D. E. *J. geophys. Res.* **92,** E641–E648 (1987).
49. Ganapathy, R. *Science* **220,** 1158–1160 (1983).
50. Smit, J. & Hertogen, J. *Nature* **285,** 198–200 (1980).
51. Kyte, F. T., Zhou, Z. & Wasson, J. T. *Nature* **288,** 651–656 (1980).
52. Crocket, J. H. & Kuo, H. Y. *Geochim. cosmochim. Acta* **43,** 831–842 (1979).
53. Harriss, R. C., Crocket, J. H. & Stainton, M. *Geochim. cosmochim. Acta* **32,** 1049–1056 (1968).
54. Kelley, V. C. *U.S. geol. Surv. Bull.* **1689A,** (1986).
55. Paul, D. K., Crocket, J. H. & Nixon, P. H. in *Kimberlite Diatremes and Diamonds: Their Geology, Petrology and Geochemistry,* Vol. 1 (eds Boyd, F. R. & Meyer, H. O. A.) 272–279 (Am. geophys. Un., Washington, 1979).
56. Winchester, J. A. & Floyd, P. A. *Chem. Geol.* **20,** 325–343 (1977).
57. Kirchner, E. *Mitt. Österr. geol. Ges.* **71/72,** 385–396 (1980).
58. Brookins, D. G. & Lambert, S. J. *Mat. Res. Soc. Symp. Proc.* **112,** 233–241 (1988).
59. Cassinis, G., Giobbi, E., Neri, C. & Ori, C. G. in *Field Conference on Permian and Permian-Triassic Boundary in the South-Alpine Segment of the Western Tethys, Field Guide-Book* 151–166 (Soc. Geol. Ital., Brescia, Italy, 1986).
60. D'Amico, C. in *Field Conference on Permian and Permian-Triassic Boundary in the South-Alpine Segment of the Western Tethys, Field Guide-Book* 16–22 (Soc. Geol. Ital., Brescia, 1986).
61. Kucha, H. *Tschermak's Miner. Petrogr. Mitt.* **28,** 1–16 (1981).
62. Kucha, H. *Econ. Geol.* **77,** 1578–1591 (1982).
63. Kucha, H. *Trans. Inst. Mining Metall.* **92,** B72–B79 (1983).
64. Goodfellow, W. D. *Chem. Geol. Isotope Geosci. Sec.* **65,** 359–382 (1987).
65. Wilde, P. & Berry, W. B. N. in *Nature and Origin of Cretaceous Carbon Rich Facies* (eds Schlanger, S. O. & Cita, M. B.) 209–224 (Academic, New York, 1982).
66. Macdougall, J. D. *Science* **239,** 485–487 (1988).
67. Kralik, M., Krumm, H. & Schramm, J. M. in *Geodynamics of the Eastern Alps* (eds Flugel, H. W. & Faupl, P.) 164–177 (Deuticke, Vienna, 1987).
68. Gromet, L. P., Dymek, R. F., Haskin, L. A. & Korotev, R. L. *Geochim. cosmochim. Acta* **48,** 2469–2482 (1984).
69. Kyte, F. T. & Wasson, J. T. *Science* **232,** 1225–1229 (1986); *Science* **234,** 1484–1486 (1986).
70. Turekian, K. K. in *Handbook of Geochemistry* (ed. Wedepohl, K. H.) Ch. 27-K, 28-K (Springer, Heidelberg, 1978).

GroE heat-shock proteins promote assembly of foreign prokaryotic ribulose bisphosphate carboxylase oligomers in *Escherichia coli*

Pierre Goloubinoff, Anthony A. Gatenby* & George H. Lorimer

Central Research and Development Department, Experimental Station, E.I. DuPont de Nemours and Co., Wilmington, Delaware 19880-0402, USA

Assembly of foreign prokaryotic ribulose bisphosphate carboxylases (Rubiscos) in Escherichia coli *requires both heat-shock proteins groEL and groES. GroEL is related to a chloroplast protein implicated in Rubisco assembly. Bacteria and chloroplasts therefore have a conserved mechanism that uses auxiliary proteins to assist in the assembly of Rubisco.*

THE subunits of some oligomeric proteins lack the inherent ability to correctly assemble into biologically functional molecules[1-4]. For the post-translational assembly of these polypeptides into oligomeric structures a ubiquitous class of conserved proteins, termed 'chaperonins', is thought to be involved[1]. This class of proteins includes the *E. coli groEL* gene product[1], as well as homologous proteins in other bacteria[5,6], chloroplasts[1], and mitochondria from plants, fungi and animals[7].

Both groEL and groES proteins are necessary for the morphogenesis of certain bacteriophages[8-12]. They are also involved in DNA replication in *E. coli*[13,14]. A molecular mechanism accounting for the involvement of the groE proteins in these processes is lacking however. The chloroplast homologue of groEL is called the Rubisco-binding protein because of its demonstrated association with newly synthesized chloroplast-encoded Rubisco large subunits[15,16], or with subunits imported into the organelle[17]. Both GroEL and Rubisco-binding protein have a similar structure and share extensive amino-acid sequence homology[1,18]. It has been suggested that in chloroplasts the Rubisco-binding protein is involved in assembly of hexadecameric (L_8S_8) Rubisco[19-21]. Here again, a detailed molecular mechanism is wanting.

Chloroplast Rubisco is comprised of eight large subunits and eight small subunits[22]. Rubiscos with a similar structure are present in most photosynthetic prokaryotes[23]. However, another form of Rubisco, a dimer (L_2) of large subunits, exists in the prokaryote *Rhodospirillum rubrum*[24]. The dimer from *R. rubrum* is similar in structure to a pair of large subunits of chloroplast Rubisco[25-27]. The structure of the hexadecameric chloroplast enzyme can be generated by tetramerization of *R. rubrum*-like dimers, to which the eight small subunits are polarily appended[26-28]. Both the prokaryotic L_2 and L_8S_8 enzymes can be synthesized and assembled in *E. coli*[29-32]. The demonstrated homology between the *E. coli* groEL protein and the chloroplast Rubisco-binding protein[1], led us to consider the possibility that the assembly of prokaryotic Rubisco in *E. coli* involves the bacterial groEL protein.

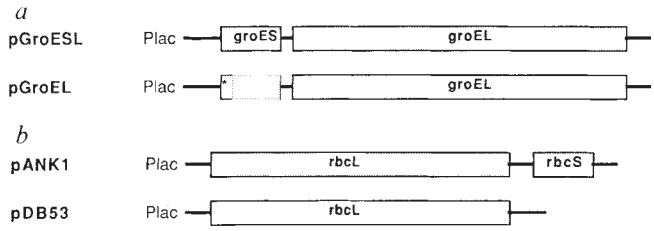

Fig. 1 Plasmid constructions. Two series of compatible plasmids were co-transformed in *E. coli* hosts. *a*, The first series (pGroESL and pGroEL) used plasmid pTG10, which has a p15A replicon, as a parent vector for the *groE* genes. pGroESL contains the *E. coli groES* and the *groEL* genes cloned in pTG10. pGroEL contains a frame-shifted (inactivated) *groES* gene followed by a wild-type *groEL* gene cloned in pTG10. *Translation frameshift. *b*, The second series of plasmids (pANK1 and pDB53) used pUC18 and pUC8 plasmids respectively, as parent vectors for the Rubisco genes. The pUC plasmids have a pMB1 replicon which is compatible with the p15A replicon. pANK1 (ref. 37) codes for both the Rubisco *rbcL* and *rbcS* genes from *A. nidulans.* cloned in pUC18 (ref. 38). pDB53 (ref. 31) codes for only the *A. nidulans rbcL* gene, cloned in pUC8 (ref. 39).
Methods. Plasmid pTG10 was derived from plasmid pACYC184 (ref. 40) which was cut with *Hin*dIII/*Bam*HI and repaired with Klenow. Into this repaired site was inserted a S1-nuclease-treated 433 base-pair *Hae*II fragment, containing the *lac* promoter and the multiple cloning site from plasmid pUC8. Plasmid pGroESL was made by cloning the *groE* operon, as a 2.3 kb *Eco*RI-*Hin*dIII fragment from plasmid pOF39 (ref. 13), into pTG10. Plasmid pGroEL was derived from a partial *Sac*II digestion of pGroESL, treated with T4 DNA polymerase. The resulting repair of the *Sac*II site located at codon 37 of *groES*[13] produced a frame-shift mutation.

Here, we show that assembly of prokaryotic dimeric (L_2), octomeric (L_8), and hexadecameric (L_8S_8) Rubiscos in *E. coli* requires both groES and groEL proteins. Although the groE proteins have been shown to mediate the assembly of L dimers from monomers, we cannot exclude subsequent involvement of these proteins in the formation of octomers and hexadecamers from these dimers.

* To whom correspondence should be addressed.